ESAIM: Proceedings, Vol. 1, 1996, pp. 241–253
http://www.emath.fr/proc/Vol.1/

Finite-Dimensional Description of Non-Newtonian Vortex Flows

Roger E. Khayat
National Research Council of Canada
Industrial Materials Institute
75, de Mortagne Blvd.
Boucherville (Qc) J4B 6YA, Canada

Abstract

The application of finite-dimensional dynamical systems theory to non-Newtonian vortex flow indicates the presence of complex temporal dynamics that is attributed to shear thinning and normal stress (giving rise to the so-called Weissenberg rod climbing phenomenon). These aspects are examined for Rayleigh-Benard thermal convection and Taylor-Couette rotational flow, in an attempt to elucidate on the mechanisms behind the onset and destabilization of secondary vortex flow common to these and possibly other non-Newtonian flows in the transition regime. Three transition scenarios are particularly explored, namely, the transition to chaos via intermittency, quasiperiodicity and period doubling.

1 Introduction

Like any flow in the transition or turbulent regime, the Rayleigh-Benard thermal convection and Taylor-Couette flow involve a continuous range of excited spatio-temporal scales. In order to assess the effect on the motion of the arbitrarily many smaller length scales, one would have to resolve in detail the motion of the small scales. This issue remains an unresolved one since, despite the great advances in storage capacity and speed of modern computers, it will not be possible to resolve all of the continuous range of length scales in turbulent flows. It is by now well established that low-order dynamical systems constitute an alternative to conventional numerical methods as we strive to understand the nonlinear behavior of flow [14]. The simplicity of the Lorenz equations and the rich sequence of flow phenomena exhibited by their solution [3, 4, 16] have been the major contributing factors to their widespread use as a model for examining the onset of chaotic motion. Despite the severe level of truncation involved in the formulation of these equations, some of the basic qualitative elements of the onset of thermal convection and the destabilization of the cellular structure have been recovered through the model. In this paper, we address the influence of non-Newtonian effects on the nature of and stability of the vortex structure in thermal convection and rotating flow by adopting a low-order nonlinear dynamical systems approach similar to the one leading to the Lorenz equations [10]. We are more particularly interested in examining the influence of shear thinning and fluid elasticity on the transition from the laminar to the turbulent regimes of non-Newtonian fluids. Our recent studies on thermal convection [5–7] and rotating flow of an Oldroyd-B fluid [8] indicate that fluid elasticity tends to have a dramatic influence on the conditions under which the base flow loses its stability to vortex flow, which in turn loses its stability as the flow approaches the transition regime. In this paper, we focus our attention on the various routes a non-Newtonian fluid may take as it evolves towards turbulence.

2 Rayleigh-Benard thermal convection

Consider a non-Newtonian fluid placed horizontally between two flat plates separated by a distance D. The x-axis is taken along the plates lying half way in between, and the z-axis is in the direction perpendicular to the plates. Let T_0 and $T_0 + \delta T$ be the temperatures of the upper and lower plates, respectively, with δT being the temperature difference. T_0 is taken as the reference temperature. We define dimensionless independent and dependent variables by introducing reference length, time, velocity and stress as D, D^2/κ, κ/D and $\eta_0\kappa/D^2$, respectively. Here κ is the thermal diffusivity of the fluid, and η_0 the zero-shear-rate viscosity. If the Boussinesq's approximation, which states that the effect of compressibility is negligible everywhere in the conservation equations except in the buoyancy term, is assumed to hold, then the equations for conservation of mass, momentum and energy, for the departure from the pure conductive state, are given in dimensionless form as [2]:

$$\nabla \cdot \mathbf{u} = 0, \qquad Pr^{-1}\left(\frac{\partial \mathbf{u}}{\partial t} + \mathbf{u}\cdot\nabla\mathbf{u}\right) = -\nabla p - \nabla\cdot\tau + \theta\mathbf{k}, \qquad \frac{\partial\theta}{\partial t} + \mathbf{u}\cdot\nabla\theta = \nabla^2\theta + Ra\mathbf{u}\cdot\mathbf{k} \quad (1)$$

where $\nabla\left(\frac{\partial}{\partial x}, \frac{\partial}{\partial z}\right)$ is the two-dimensional gradient operator in the (x, z) coordinates, $\mathbf{u}(u, w)$ is the velocity vector, p is the pressure, τ is the deviatoric stress tensor whose form is dictated by an appropriately imposed constitutive equation, $\theta = (T^* - T_S^*)/\delta T$ is the departure from the steady-state temperature T_S^*, and $\mathbf{k}$ is the unit vector along the z-direction. The following dimensionless groups have been introduced, namely the Rayleigh number and Prandtl number:

$$Ra = \frac{\delta T g \alpha_T D^3}{\kappa\nu_0}, \qquad Pr = \frac{\nu_0}{\kappa} \quad (2)$$

with ν_0 being the zero-shear-rate kinematic viscosity, α_T the coefficient of thermal expansion, and g the acceleration due to gravity. Note that the work term in the energy equation has been neglected. As to the boundary conditions, since the fluid is confined between the planes $z = -1/2$ and $z = +1/2$, regardless of the nature of the two surfaces, the temperature is taken fixed at the bounding planes, and the normal velocity component is zero. There are two remaining boundary conditions which, however, do depend on the nature of the two bounding surfaces. We assume that the two planes are free surfaces on which the tangential stress component is equal to zero.

2.1 Thermal convection of shear-thinning fluids

The derivation of the low-order dynamical system for a shear-thinning fluid follows very closely that of the Lorenz equations. In the present study, we assume that the fluid obeys the Carreau-Bird law for viscosity [1], so that τ obeys the following constitutive equation (in dimensionless form):

$$\tau = -\eta(\dot\gamma)\dot\gamma; \qquad \eta(\dot\gamma) = s + (1-s)\left[1 + (E\dot\gamma^2)\right]^{\frac{n-1}{2}} \quad (3)$$

where $E = \lambda\kappa/D^2$ is the elasticity number, λ being the relaxation time, n is the power-law exponent, which for a shear-thinning fluid is less than one, $\dot\gamma$ is the rate-of-strain tensor, and s is the ratio of zero- to infinite-shear-rate viscosities. It is assumed that E is small so that only leading order terms are retained in the binomial expansion. The solution to Eqs. 1 and 3, subject to the above boundary conditions, may be represented by an infinite Fourier series in x and z, with the series coefficients depending on time alone. Projection of the equations onto the various eigenmodes leads to an infinite set of nonlinear and coupled ordinary differential equations that govern the

coefficients. In practice, one seeks a way to truncate the Fourier series to obtain a finite-dimensional system of ordinary differential equations. The truncation, however, cannot be arbitrary since the truncated form of the solution must still satisfy the imposed boundary conditions and lead to a model physically and mathematically coherent with the initial equations. In the present work, an additional restriction imposes itself naturally on the truncated solution: the resulting dynamical system must reduce to the Lorenz equations in the limit of a Newtonian fluid as $E \to 0$. However, there is an additional difficulty in the present case because of the nonlinear dependence of the viscosity on shear rate. The presence of the nonlinearity in expression (3) would make the derivation of the desired ordinary differential equations governing the coefficients extremely difficult (if at all possible) if the projection were attempted. In order to make the problem more tractable, we carry out the binomial expansion in (3), and take E small enough to guarantee convergence. The present formulation and subsequent numerical results are thus limited to flows at moderately small shear rate or relaxation time. This assumption is not unreasonable since, although large strains may be present during thermal convection, only small shear rates are usually involved. Thus, keeping terms to $O(E^2)$, the binomial expansion of Eq. 3, and in a manner similar to the case of a Newtonian fluid [10, 15], we retain only one term in the Fourier representation for the streamfunction and two terms for the temperature. This insures that some part of the convective nonlinearities is retained from the energy equation. The three resulting time-dependent coefficients are thus governed by the following three-dimensional system:

$$\dot{X} = Pr\left[Y - X - (n-1)c(q)E^2X^3\right], \qquad \dot{Y} = -XZ + rX - Y, \qquad \dot{Z} = XY - bZ \tag{4}$$

where q is the period along the x direction, and a dot denotes the $\tau d/dt$ operation. As in the case of the Lorenz equations, the following parameters were also introduced:

$$r = q^2\tau^3 Ra, \qquad b = 4\pi\tau, \qquad \pi = \frac{1}{\pi^2 + q^2} \tag{5}$$

Finally, the $c(q)$ factor in Eqs. 4 is given by

$$c(q) = \left(\frac{\sqrt{2}}{\pi q}\right)^3 \left[\frac{1}{\pi^2}\left(\frac{9}{32\tau^2} - \frac{\pi^2 q^2}{2}\right) + 4(\pi^4 + q^4)\left(\frac{3}{16\tau^2} - \pi^2 q^2\right)\right] \tag{6}$$

In the limit $E \to 0$, that is in the case of a Newtonian fluid, Eqs. 4 reduce to the Lorenz equations [10]. It is important to observe that the nonlinearities in the non-Newtonian equations (4) stem from the convective terms as in the Lorenz equations, and from the viscous terms resulting from the shear-rate dependence of viscosity. This is in contrast to the case of a viscoelastic fluid where the type of nonlinearity is the same as in the Lorenz equations.

We now turn to the local stability of the equilibrium branches of solution in an attempt to elucidate on some of the fundamental differences between Newtonian and shear-thinning fluids. As in the case of the Lorenz equations, there is one trivial fixed point (the origin in phase space) which corresponds to pure heat conduction. As r exceeds unity, two additional fixed branches, C_1 and C_2, emerge, corresponding to the onset of (two-dimensional) convective rolls in opposite directions. Stability analysis of the conductive state is exactly the same as in the case of the Lorenz equations. The corresponding eigenvalues are always real since $r > 0$, and one of them becomes positive as soon as r exceeds one. That is when the origin loses its stability to the two other steady-state solution branches. Thus, the critical value of the Rayleigh number at the onset of (steady two-dimensional) convection does not depend on E. In other words, at least on the basis of the present model, *the critical Rayleigh number and wavenumber at the onset of the cellular structure for a non-Newtonian*

fluid is the same as those for a Newtonian fluid. This important conclusion is expected since the effect of the nonlinear terms, in particular the viscous cubic term, is not felt in the vicinity of the conductive state which is a state of rest. This result is in agreement with the experiments of Liang and Acrivos [9] and is the same for an Oldroyd-B fluid [5, 6]. The neutral stability curve in the (Ra, q) plane is then the same as the one predicted by linear stability analysis of the exact equations (1) and (3), and is given by $Ra = [(\pi^2 + q^2)^3]/q^2$, so that the critical wavenumber for the most unstable mode is equal to $q_c = \pi/\sqrt{2}$, corresponding to a minimum value of the Rayleigh number $Ra_c = \pi^4/27$. The bifurcation branches and stability are shown in Fig. 1 for $E \in [0., 0.04]$ and $n = 0.2$. At very small E value, the qualitative behavior of the solution amplitude as function of r is the same as that for a Newtonian fluid, except that the amplitude tends to grow with E. Thus, shear thinning tends to give rise to larger rolls. As E increases, the monotonic growth of the amplitude gives way to that shown in Fig. 1. If we refer to the curve corresponding to $E = 0.02$, we see, typically, that beyond some r value, a non-trivial steady-state solution does not exist. In order to assess the impact of shear thinning on the solution in phase space, we examine first the general stability of the two branches C_1 and C_2. The stability in the vicinity of the critical point $r = 1$ must be analyzed separately; this analysis will be carried out in a future paper using the center manifold theorem. For small E, linear stability analysis around C_1 and C_2 leads to an exchange of stability which takes place at $r = 1$ similarly to the Lorenz solution. At $r = 1$, a supercritical bifurcation emerges as shown in Fig. 1. The conductive state, which is stable for $r < 1$, loses its stability to the two convective branches as r exceeds unity. Thus, for $r > 1$, the solution evolves to either one of the branches depending on the initial conditions. As r increases and reaches a critical value $r_h(E, Pr, n) > 1$, the two convective states lose their stability through a Hopf bifurcation. In this case, the solution tends to "hover" from around one branch to the other passing through the origin, and eventually remains locked (in phase space) on what is now well established as the strange attractor. This situation persists as long as E remains very close to zero. As E increases, the branches C_1 and C_2 indicate the presence of a turning point that tends to coincides with the onset of a Hopf bifurcation. The analysis around the turning point is involved, and the resulting dynamics is complicated and thus is left for future investigation.

The following calculations are conducted for a fluid with a Prandtl number $Pr = 7$, and $b = 8/3$. We focus our attention to the influence of inertia on the onset and stability of thermal convection by varying the Rayleigh number for a fixed level of shear-thinning. We thus set the value of E in Eqs. 4 equal to 0.008. This value typically corresponds to fluids of moderately low level of shear thinning. Many of the supposedly Newtonian fluids may have an E value of $O(10^{-3})$. In the precritical range $(r < r_c = 1)$, the solution of Eqs. 4, in the vicinity of the origin, decays exponentially to the origin. Numerical integration confirms this result and shows that the origin is globally (asymptotically) stable. We shall therefore concentrate our attention on the more interesting postcritical range, i.e., $r > r_c$. We examine the flow as the Rayleigh number is increased further. For $r \in [1, 22]$ the behavior of flow is essentially similar to that for a Newtonian fluid as described above, with the flow remaining chaotic for an r value of up to 22 when the flow begins to exhibit some regularity. For r between 22 and 23, the flow undergoes complex dynamical behavior that is not easy to classify. Thus, at $r = 22.99$, the flow begins to show a more coherent and even periodic structure There is considerable thinning of the band width of the attractor in phase space, and some of the more dominant frequencies begin to appear in the power spectrum. The flow begins to undergo an inverse sequence of period doubling as r is increased further, with $r = 22.99$ corresponding roughly to the cumulation point. As r is increased further, the number of periods decreases. Complete periodic behavior is observed at $r = 23$, but the motion becomes chaotic again for $r \in]23, 23.1]$. Periodic or possibly quasiperiodic behavior is restored at roughly $r = 23.1$, with the temporal behavior and phase trajectory exhibiting distortion due to nonlinear effects. As r increases, the period decreases

when the motion is of period 4 at $r = 23.15$. The period-2 motion occurs at $r = 23.2$. The basic periodic motion is depicted at $r = 23.3$. There is only one fundamental frequency and its harmonics in the power spectrum. As r increases, the motion remains periodic with the distortion of the limit cycle slowly disappearing, giving way to a completely symmetric periodic orbit at $r = 26.5$. This periodicity is, however, broken as r is increased further leading to intermittent motion.

In general, a signal is called intermittent if it is subject to infrequent variations of large amplitude [12]. For a value of r less than $r_i = 26.5$, the dynamical system (4) has a stable limit cycle as indicated by the velocity time signature in Fig. 2a. The solution oscillates in a regular fashion and is stable against small perturbations. When r slightly exceeds r_i (the intermittency threshold), we have an intermittent dynamical regime as shown in Fig. 2b for $r = 26.54$. The time signal in the figure consists of oscillations that appear regular and that resemble the stable oscillatory behavior for $r \leq r_i$. But now, the oscillations are interrupted from time to time by *abnormal* fluctuations or turbulent bursts, whose amplitude and direction are approximately the same from one fluctuation to another, and that depend little on r as depicted from Figs. 2c and 2d. These figures corresponding, respectively, to $r = 26.55$ and 26.57, show clearly that it is neither the amplitude nor the duration of the exceptional fluctuations that tend to increase as r increases from r_i, but only their average frequency. These erratic fluctuations have a well-defined average duration and terminate by relaminarization, i.e., a return to the laminar regime. This description corresponds to transition via intermittency of type-I [12, 13].

2.2 Thermal convection of viscoelastic fluids

We examine the thermal convection of an upper-convected Maxwell fluid. In this case, the constitutive equation for the deviatoric stress tensor is given by:

$$\frac{\partial \tau}{\partial t} + \mathbf{u} \cdot \nabla \tau - \nabla \mathbf{u}^t \cdot \tau - \tau \cdot \nabla \mathbf{u} = -E^{-1}(\tau + \dot{\gamma}) \tag{7}$$

The corresponding dynamical system is derived elsewhere [5], and therefore the details are not given here. Thus, taking one Fourier component in the streamfunction, two for the temperature and one for the stress, with corresponding coefficients X, Y and Z, and P, respectively, one obtains the following four-dimensional dynamical system:

$$\dot{X} = Pr(Y - P), \qquad \dot{Y} = -XZ + rX - Y, \qquad \dot{Z} = XY - bZ, \qquad \dot{P} = \tau E^{-1}(X - P) \tag{8}$$

where the parameters are the same as in Eqs. 4. Note that in the limit $E \to 0$, one also recovers the Lorenz equations. It is interesting to observe that the nonlinearities in this case, unlike Eqs. 4, are of purely convective origin, and are the same as those in the Lorenz equations. The results based on linear stability analysis of Eqs. 8 are summarized in Fig. 3. Linear stability analysis around the origin leads to an obvious characteristic value: $\lambda = -b$, while the remaining three roots indicate that at small E value, there is a sn exchange of stability similar to the cases of shear thinning and Newtonian fluids, which takes place at $r = 1$ when a supercritical bifurcation emerges as shown in Fig. 1. The conductive state, which is stable for $r < 1$, loses its stability to the two convective branches as r exceeds unity. The emergence of the branches C_1 and C_2 corresponds to the onset of steady convection. Thus, for $r > 1$, the solution evolves to either one of the branches depending on the initial conditions. As r increases and reaches a critical value $r_h(E, Pr) > 1$, the two convective states lose their stability through a Hopf bifurcation. This situation persists as long as E remains smaller than a critical value, namely, $E^c = \tau(Pr + 1)/Pr$.

As E exceeds E^c, stability analysis around $r = 1$ shows that both the origin and the two convective branches are unstable [6] as shown in Fig. 3. In the range $r < 1$, a Hopf bifurcation

emerges at $r = r^h(E, Pr)$, corresponding to the onset of overstability or periodic solution. The origin was found to be stable for $r < r^h$, and unstable for $r > r^h$. Thus, the solution would evolve towards the conductive state in the former case, while it ends up on a periodic orbit in the latter. The stability of the periodic orbit was later confirmed by applying the center manifold theorem around $r = r^h < 1$ [7]. Note that although the birth of the Hopf bifurcation occurs at a precritical r value ($r^h < 1$), a limit cycle usually exists for the solution at $r > 1$. Thus, when $E > E^c$, the branches C_1 and C_2 are always unstable, and the solution settles into periodic orbit even after r has exceeded unity. Thus, *for strongly elastic fluids, steady convection cannot set in when the Rayleigh number exceeds* Ra_c. This is of course in sharp contrast to the case of weakly elastic fluids ($E < E^c$), including Newtonian and shear-thinning fluids, where steady convection always sets in as Ra exceeds Ra_c. Multiple-scale stability analysis [6] indicate that steady-state convection can lose its stability at $r = r_h$ to periodic motion via a Hopf bifurcation. Such an exchange of stability is not permitted in the case of Newtonian or shear-thinning fluid. Periodic motion sets in, however, if the level of elasticity exceeds a critical value $E_h < E^c$. We now turn to some numerical results confirming this behavior.

We fix $Pr = 10$, and in this case $E_h = 0.01$. We thus fix the value of $E = 0.022$. One then expects to observe a limit cycle at $r_h = 3.65$ of initial (dimensionless) angular frequency $\omega = 4.747$ [6]. For $r = 3.9$, the fundamental frequency is of (dimensionless) value equal to 0.68 compared to the value $\omega/2\pi = 0.76$ predicted by theory [6]. The difference is due to nonlinear effects. These nonlinearities give rise to the distortion in the periodic orbit (not shown) and the additional harmonics. When r exceeds a certain critical value, the periodic orbit (around C_1, say) begins to lose its stability. The trajectory is attracted toward another periodic orbit (around C_2) in a manner similar to homoclinic bifurcation. Further increase in r leads to complete instability of the periodic motion around C_1 and C_2. Figure 4a illustrates the beginning of loss of periodicity at $r = 4.1$ which is accompanied by a weak modulation in the time signal (not shown). The loss of periodicity becomes clearer when r increases further. Figure 4b shows the quasi-periodic solution at $r = 4.3$. Additional amplitude modulation is observed, although weak, as indicated by the power spectrum in the figure. There is a second fundamental frequency $f_2 < f_1$ with a slight shift in the f_1 value to the right. The spectrum shows peaks at the combination frequencies of $mf_1 + nf_2 (m, n = 0, \pm 1, \pm 2, \ldots)$. At $r = 4.4$, a third fundamental frequency f_3 emerges in the power spectrum in Fig. 4c accompanied by a broadening around f_1 and f_2, thus indicating the onset of weak chaotic behavior as can be confirmed from the broadening of the power spectrum base. The power spectrum in Fig. 4d shows a significant decrease in amplitude and additional broadening at the fundamental frequency f_1. The third fundamental frequency f_3 disappears together with the higher harmonics.

3 Taylor-Couette flow of a viscoelastic fluid

We consider an incompressible viscoelastic fluid confined between two infinite and concentric cylinders of inner and outer radius R_i and R_o, respectively. The inner cylinder is taken to be rotating at an angular velocity Ω, while the outer cylinder is at rest. The fluid is assumed to obey the upper-convected Maxwell equation which, in non-dimensional form, is given by Eq. 7. The derivation of the corresponding dynamnical system, in this case involving six degrees of freedom, is detailed elsewhere [8]. The conservation and constitutive equations as well as the boundary conditions are first obtained for axisymmetric flow in the narrow-gap limit. These equations are solved by assuming an infinite discrete Fourier representation in space for the flow field, which, upon truncation, leads

to the following finite dynamical system that governs the expansion coefficients:

$$\begin{gathered}\dot{U} = V + X, \qquad \dot{V} = -UW + rU + Y, \qquad \dot{W} = UV + bZ, \\ \dot{X} = -\tau E^{-1}(X + U), \qquad \dot{Y} = -bUZ - \psi WX - rX - \tau E^{-1}(Y + V), \\ \dot{Z} = \beta UY - \beta\psi VX - \tau E^{-1}(Z + W).\end{gathered} \tag{9}$$

where (if we let $D = R_o - R_i$)

$$E = \frac{\lambda\nu_0}{D^2}, \qquad r = q^2\tau^3\left(\frac{D}{R_i}\right)\left(\frac{R_i\Omega D}{\nu_0}\right)^2, \qquad \beta = \frac{1}{b}, \qquad \psi = \tau(3\pi^2 - q^2). \tag{10}$$

In this case, U, V and W are related to the Fourier representation of velocity, and X, Y, and Z are related to the stress coefficients. Note that q is the wavenumber imposed in the axial direction. In the limit $E \to 0$, that is, in the case of a Newtonian fluid, Eqs. 16–21 reduce to the Lorenz equations (9) with the Prandtl number equal to one.

For small E, stability analysis of Eqs. 9 leads to an exchange of stability similar to the case of a Newtonian fluid, which takes place at $r = r_c(E)$, except that, unlike thermal convection, the critical value r_c now depends strongly on fluid elasticity and is different from one. At $r = r_c$, a supercritical bifurcation emerges. The base flow, which is stable for $r < r_c$, loses its stability to the two steady branches C_1 and C_2 as r exceeds r_c. As r increases and reaches a critical value, the two branches lose their stability. This stability and bifurcation picture remains essentially unchanged until E exceeds a critical value, E^{sub} say, when the supercritical bifurcation gives way to a subcritical bifurcation at $r = r_c$. The influence of the elasticity number on the bifurcating branches at $r = r_c$ is shown in Fig. 5 for $q = 6$. There are several important aspects to be observed from Fig. 5, in contrast to the Taylor-Couette flow of a Newtonian fluid. We first observe the strong dependence of r_c on fluid elasticity. For small E, there is a supercritical bifurcation at $r = r_c$, with r_c becoming increasingly smaller as E increases, and decreasing all the way to zero. At the critical value $E = E^{\text{sub}}(q)$, which in this case ($q = 6$) is equal to 0.014, the bifurcation changes from super- to subcritical. This corresponds to a change in concavity at ($r = r_c$, $U_s = 0$). In the supercritical regime, when $r < r_c$, a small disturbance of the base flow decays exponentially according to linear theory. The nonlinear terms in Eqs. 9 remain small in this case. This situation remains essentially unchanged as the initial flow disturbance and thus nonlinear effects increase. As r exceeds r_c, linear theory predicts an exponential growth of a small disturbance of the base flow. This growth, however, is halted by the stabilizing nonlinear effects. Although linear theory may describe well the onset of secondary flow, it fails to give the magnitude of the steady disturbance. In the subcritical regime ($E > E^{\text{sub}}$), when $r < r_g$ (shown here for the curve $E = 0.05$), the flow is globally asymptotically stable [13]. When $r_g < r < r_c$, two bifurcation solutions exist for the disturbance from the base flow. In this case, any disturbance below a certain threshold decays to the origin. Above the threshold value, the base flow is destabilized. In this range of r values, the flow is commonly defined as metastable [11]. Whether the bifurcation at r_c is subcritical or supercritical, the TVF loses its stability at some critical r value $r_h > r_c$ (shown here for the curve $E = 0.05$). We turn our attention to the influence of inertia when the elasticity number exceeds the critical value E^{sub}. For such a flow, the onset of TVF coincides with the birth of a subcritical bifurcation as depicted from Fig. 5. We examine the flow for $E = 0.05$. Figure 5 indicates that $r_c = 0.3$. From linear stability analysis, the TVF appears to be unstable for $0.2 < r < 0.3$, stable for $0.2 < r < 0.54$, and unstable again for $r > 0.54$. In the range $0.2 < r < 0.3$, the base flow is stable only to small perturbation, making it possible for TVF to set in if the perturbation is large enough. This is in contrast to the situation of a weakly elastic flow, with no possibility for TVF to set in as long as r does not exceed r_c. We are particularly interested in the flow behavior after all fixed points have lost their stability, that is after the onset of the Hopf

bifurcation at $r_h = 0.54$. The flow does not seem to undergo a homoclinic bifurcation similarly to weakly elastic flows. At $r = 0.8$, Fig. 6a shows the trajectory in the (U, V) plane after transients have died out. The flow is locked in a periodic orbit as is confirmed from the corresponding power spectrum. The latter exhibits a fundamental frequency at $f = 0.2$ with three significant harmonics, reflecting the presence of nonlinearities in the temporal behavior. These nonlinear effects become more pronounced as r is increased further. At $r = 1$, there is a period doubling in the periodic solution which is depicted in the phase plane in Fig. 6b, and the emergence of subharmonics in the power spectrum. The power spectrum shows a fundamental frequency at $f/2$ with four even harmonics. This bifurcation sequence continues as r is further increased as can be observed from Fig. 6c which shows the fundamental frequency at $f/4$ for $r = 1.02$. Each subharmonic bifurcation doubles the number of sharp frequency components, and each pairwise rejoining broadens every other sharp spike. The doubling process, however, reaches an accumulation point, at roughly $r_\infty = 1.0335$, and is succeeded by a qualitatively different spatio-temporal behavior of flow. The attractor in phase space and the Fourier spectrum in fig. 6d indicate the presence of chaotic motion. The transition to chaotic behavior is rather sudden, and is accompanied by a dense orbit in phase space and a broadening in the Fourier spectrum base. Similarly to the case of the Rössler attractor, the present transition exhibits sharp frequency components in the chaotic attractor. The spectrum still displays the sharp fundamental and some of its harmonics.

References

[1] Bird, R.B., Armstrong, R.C. and Hassager, O., Dynamics of Polymeric Liquids, vol. 1, 2nd Ed., John Wiley & Sons, New York 1987.

[2] Chandrasakhar, S., Hydrodynamic and Magnetohydrodynamic Instability, Dover, New York, 1961.

[3] Jackson, E.A., Perspectives of Nonlinear Dynamics, vols. 1 and 2, Cambridge University Press, 1991.

[4] Kaplan, J.L. and Yorke, J.A., "Preturbulence: A Regime Observed in the Fluid Flow Model of Lorenz," *Comm. Math. Phys.*, **63**, pp. 93, 1979.

[5] Khayat, R.E., "Chaos and Overstability in the Thermal Convection of Viscoelastic Fluids," *J. Non-Newt. Fluid Mech.*, **53**, pp. 227, 1994.

[6] Khayat, R.E., "Fluid Elasticity and the Onset of Chaos in Thermal Convection," *Phys. Rev. E*, **51**, pp. 380, 1995.

[7] Khayat, R.E., "Nonlinear Overstability in the Thermal Convection of Viscoelastic Fluids," *J. Non-Newt. Fluid Mech.*, **58**, pp. 331, 1995.

[8] Khayat, R.E., "Onset of Taylor Vortices and Chaos in Viscoelastic Fluids," *Phys. Fluids* (in press).

[9] Liang, S.F. and Acrivos, A., "Experiments on Buoyancy Driven Convection in Non-Newtonian Fluid," *Rheol. Acta*, **9**, pp. 447, 1970.

[10] Lorenz, E.N., "Deterministic Nonperiodic Flows," *J. Atmos. Sci.*, **20**, pp. 130, 1963.

[11] Normand, C. and Pomeau, Y., "Convective Instability: A Physicist's Approach," *Rev. Mod. Phys.*, **49**, pp. 581, 1977.

[12] Pomeau, Y. and Manneville, P., "Intermittent Transition to Turbulence in Dissipative Dynamical Systems," *Comm. Math. Phys.*, **74**, pp. 189, 1980.

[13] Schuster, H.G., Deterministic Chaos, VCH Verlagsgesellschaft, Weinheim, 1989.

[14] Sell, G.R., Foias, C. and Temam, R., Turbulence in Fluid Flows: A Dynamical Systems Approach, Springer-Verlag, New York, 1993.

[15] Shirer, H.N. and Wells, R., Mathematical Structure of the Singularities at the Transitions Between Steady States in Hydrodynamic Systems, Springer-Verlag, Heidelberg 1980.

[16] Sparrow, C., The Lorenz Equations, Springer-Verlag, New York, 1983.

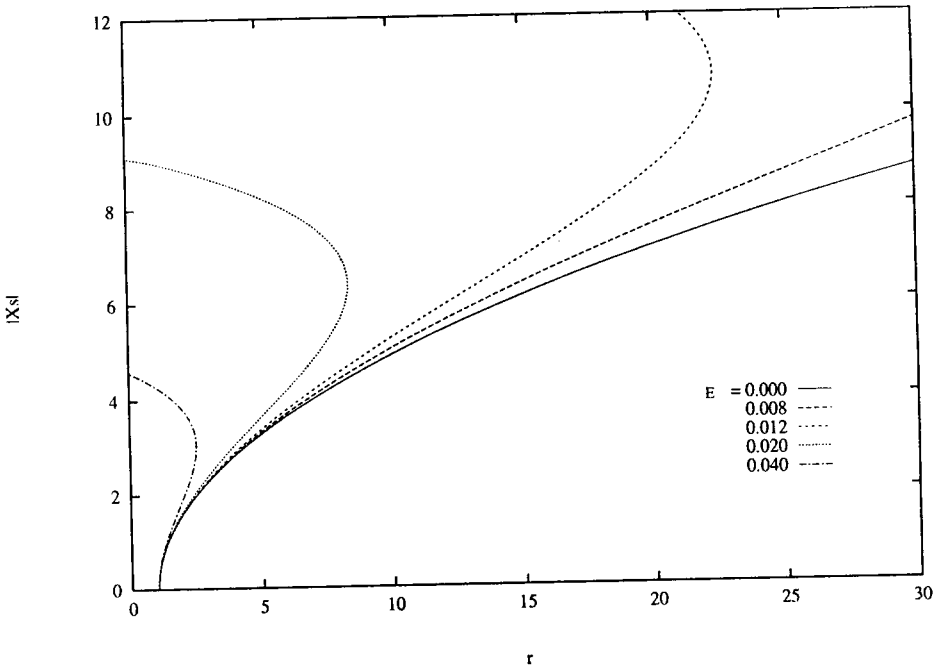

Figure 1: Bifurcation diagrams for a shear thinning fluid for various values of E.

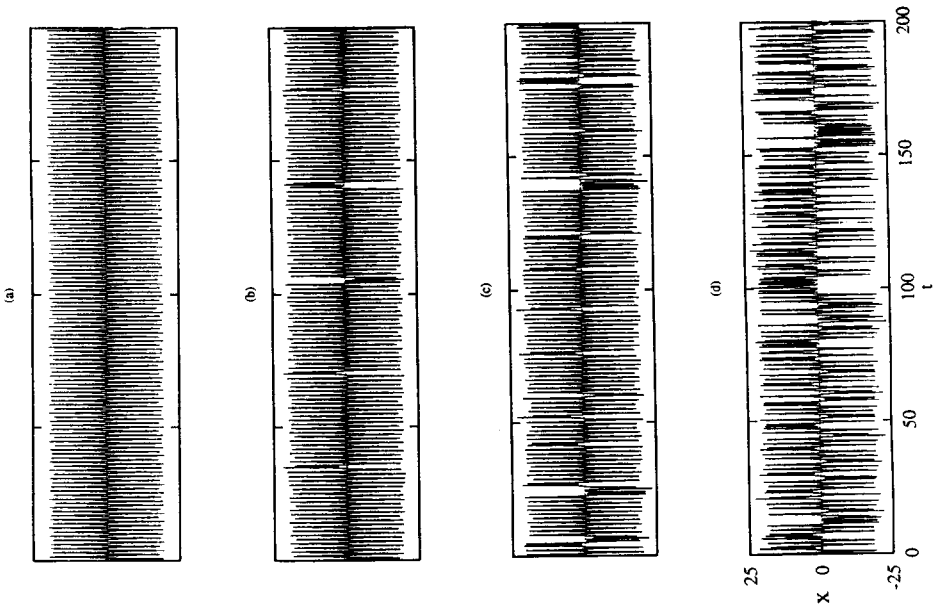

Figure 2: Intermittency route to chaos under the influence of inertia. Periodic motion at $r = 26.5$ (a), beginning of intermittent behavior at $r = 26.54$ (b), $r = 26.55$ (c), and chaotic motion at $r = 26.57$ (d).

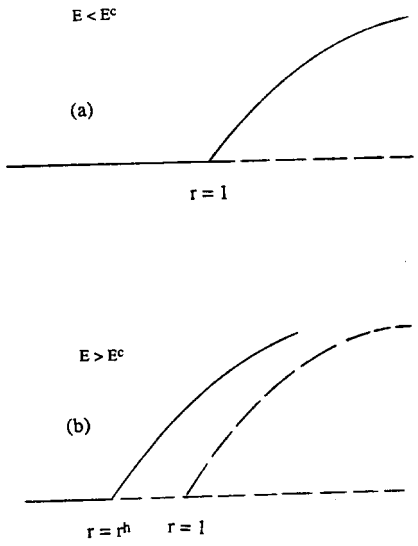

Figure 3: Schematic bifurcation diagrams around the conductive state for (a) weakly elastic flow ($E < E^c$) and (b) strongly elastic flow ($E > E^c$). Stable and unstable solution branches are indicated by solid and dashed lines, respectively. Note the birth of a precritical Hopf bifurcation (at $r = r^h < 1$) when $E > E^c$. In this case, no steady convection sets in.

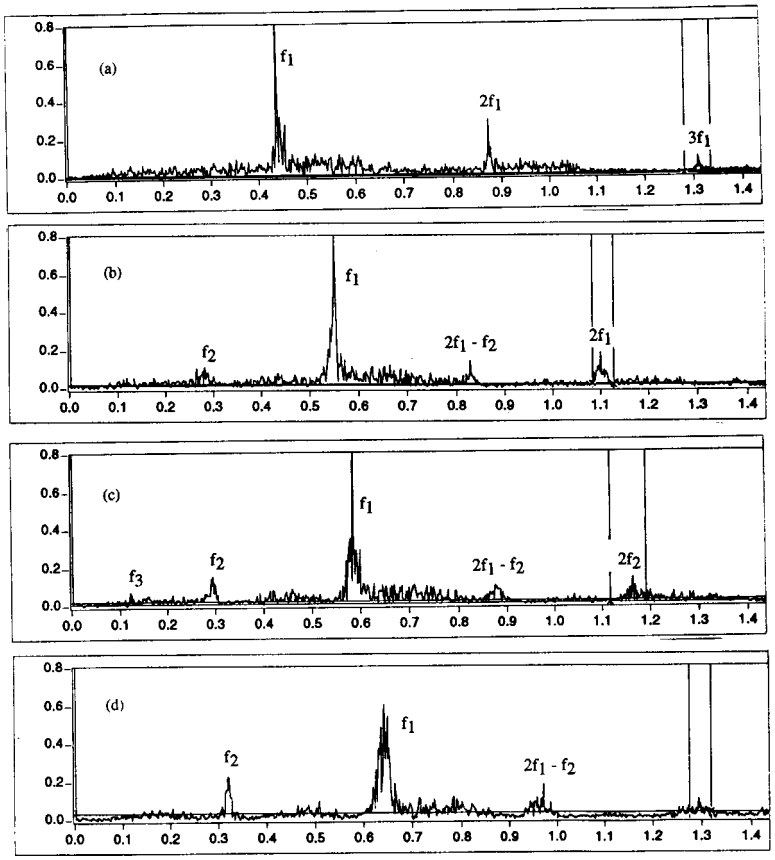

Figure 4: Quasiperiodical route to chaos for $E = 0.022$ and $Pr = 10$. Beginning of loss of periodicity at $r = 4.1$ (a), quasiperiodicity at $r = 4.3$ with two fundamental frequencies (b), quasiperiodicity at $r = 4.4$ with three fundamental frequencies (c), and chaotic motion at $r = 4.6$ (d).

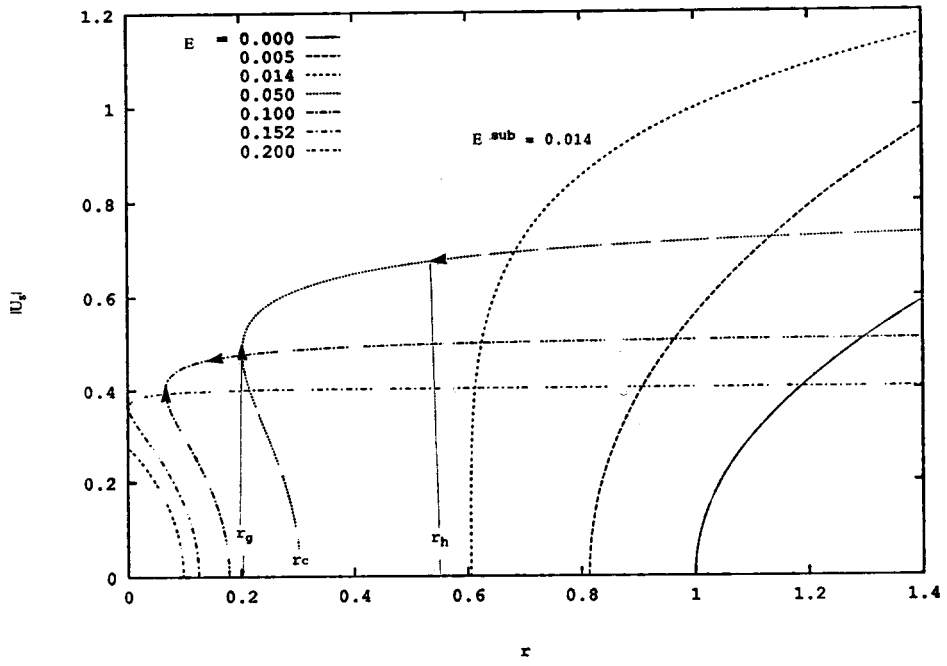

Figure 5: Bifurcation diagrams and their stability for a UCM fluid ($q = 6$). Super- and subcritical bifurcations for weakly and strongly elastic flows, respectively. Unstable regions are indicated by breaks in the lines and are delimited by two arrows. Note that for (roughly) $E > 0.1$, the TVF remains unstable.

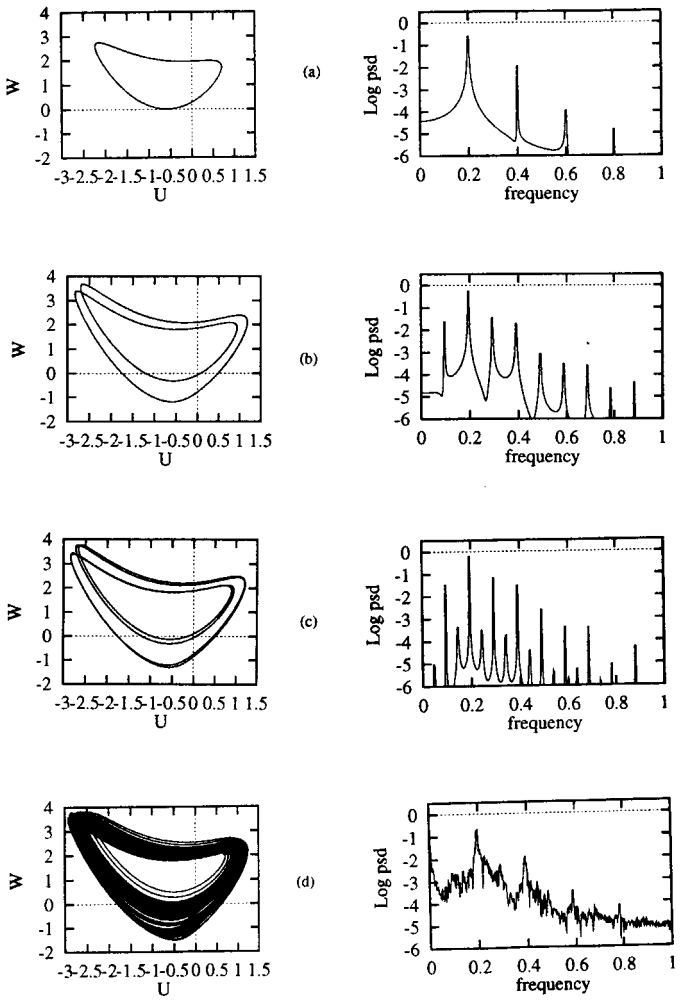

Figure 6: Period-doubling route to chaos for $E = 0.05$ and $q = 6$. Periodic motion at $r = 0.8$ (a), period-2 motion at $r = 1.0$ (b), period-4 motion at $r = 1.02$ (c), and chaotic motion at $r = 1.0335$ (d).